

Disorder induced phase transition in magnetic higher-order topological insulator: A machine learning study

Zixian Su(苏子贤), Yanzhuo Kang(康艳卓), Bofeng Zhang(张博峰), Zhiqiang Zhang(张智强), Hua Jiang(江华)
Citation: Chin. Phys. B . 2019, 28(11): 117301 . **doi:** 10.1088/1674-1056/ab4582
Journal homepage: http://cpb.iphy.ac.cn; http://iopscience.iop.org/cpb

What follows is a list of articles you may be interested in

Disorder effects in topological states: Brief review of the recent developments

Binglan Wu(吴冰兰), Juntao Song(宋俊涛), Jiaojiao Zhou(周娇娇), Hua Jiang(江华)
Chin. Phys. B . 2016, 25(11): 117311 . **doi:** 10.1088/1674-1056/25/11/117311

Fractional-dimensional approach for excitons in GaAsfilms on $Al_xGa_{1-x}As$ substrates

Zhen-Hua Wu(武振华), Lei Chen(陈蕾), Qiang Tian(田强)
Chin. Phys. B . 2016, 25(3): 037310 . **doi:** 10.1088/1674-1056/25/3/037310

A dual-band flexible frequency selective surface with miniaturized elements and maximally flat (Butterworth) response

Wang Xiu-Zhi, Gao Jin-Song, Xu Nian-Xi, Liu Hai
Chin. Phys. B . 2014, 23(4): 047303 . **doi:** 10.1088/1674-1056/23/4/047303

The effect of a non-aligned unit on double-screen frequency-selective surface transmission characteristics

Wang Jian-Bo,Lu Jun,Sun Guan-Cheng,Chen Xin-Yi,Chen Gui-Bo
Chin. Phys. B . 2012, 21(4): 047304 . **doi:** 10.1088/1674-1056/21/4/047304

Disorder induced phase transition in magnetic higher-order topological insulator: A machine learning study*

Zixian Su(苏子贤)[1], Yanzhuo Kang(康艳卓)[2], Bofeng Zhang(张博峰)[1], Zhiqiang Zhang(张智强)[1,†], and Hua Jiang(江华)[1,3]

[1] School of Physics and Technology, Soochow University, Suzhou 215006, China
[2] College of Physics and Electronic Science, Changsha University of Science and Technology, Changsha 410114, China
[3] Institute for Advanced Study, Soochow University, Suzhou 215006, China

(Received 10 June 2019; revised manuscript received 12 September 2019; published online 18 October 2019)

Previous studies presented the phase diagram induced by the disorder existing separately either in the higher-order topological states or in the topological trivial states, respectively. However, the influence of disorder on the system with the coexistence of the higher-order topological states and other traditional topological states has not been investigated. In this paper, we investigate the disorder induced phase transition in the magnetic higher-order topological insulator. By using the convolutional neural network and non-commutative geometry methods, two independent phase diagrams are calculated. With the comparison between these two diagrams, a topological transition from the normal insulator to the Chern insulator is confirmed. Furthermore, the network based on eigenstate wavefunction studies also presents a transition between the higher-order topological insulator and the Chern insulator.

Keywords: disorder effects, convolution neural network, higher-order topological states

PACS: 05.70.Fh, 72.80.Ng, 03.65.Vf **DOI:** 10.1088/1674-1056/ab4582

1. Introduction

The theory of topological states has been greatly developed since the discovery of the quantum Hall effect by Klitzing[1,2] 40 years ago. By now physicists have proposed a variety of novel topological states, including topological insulator,[3–8] topological semimetal,[9,10] topological superconductor,[11–14] and axion insulator.[15,16] The nontrivial boundary or surface states of these systems give topological states the non-dissipated channel and other transport properties that traditional materials do not have. In the past two years, the higher-order topological states[17–22] have received a lot of attention. Different from the traditional topological insulator, the higher-order topological insulator has a $d-n$ dimensional topological surface state, where d is the dimension of the system and n is the order of the higher-order topological state. When $n=1$, it corresponds to the general topological state. For $n>1$, it is generally referred as the higher-order topological state. Taking two dimensions (2D) as an example, the traditional 2D system has a band gap without elementary excitation. On the contrary, in the higher-order systems, the spectrum of the edge state needs to be opened[17–19] and 0D topological corner states are generated inside the band gap. The initial models usually have the mirror or quadruple rotation symmetry, which ensures that the edges (surfaces) of the samples have a mass domain wall[23] structure. With the proposal of the initial theoretical model,[24] the topological corner state was also confirmed in experiments.[25] Subsequently, a series of experiments also proved the diversity of higher-topological states.[23,26–28]

With the development of topological materials in condensed matter physics, the disorder effects on topological states attract a lot of research interest.[29–43] The conventional numerical characterization methods include transport simulation,[29,35,44] local current distribution simulation,[30,44] and topological index calculation.[34,37,40,41] However, these methods all have limitations in the study of the higher-order topological insulators. For example, the quantized conductance without fluctuation and the local current distribution can demonstrate the existence of edge (surface) states as well as the topological properties of a topological insulator. However, due to the presence of a 0D bound state, the topological properties of the second-order topological insulator system cannot be characterized by the transport simulation and local current distribution. Although a one-dimensional system also presents the 0D bound state, one can calculate the winding number[37,41] to separate the trivial state from the topological one. The winding number, however, cannot be directly used in a higher-order topological system with 0D bound states. Thus, there exsits an urgent need to explore new methods to study the disorder effect on the higher-order topological states.

In the past few years, machine learning has gained great development and wide applications, especially in the field of image classification. Image classification, which has sufficiently high accuracy[45] based on the convolutional neural

*Project supported by the National Natural Science Foundation of China (Grant No. 11822407) and the Priority Academic Program Development of Jiangsu Higher Education Institutions, China.

†Corresponding author. E-mail: zqzhang2018@stu.suda.edu.cn

© 2019 Chinese Physical Society and IOP Publishing Ltd

network, is also used in the research of condensed matter physics.[46–54] Since the wave function distributions for different topological phases are distinguished, machine learning should be useful to determine the 0D bound states, which will make up for the shortcomings of the traditional methods. Most recently, Araki and his collaborators firstly studied the disorder induced phase transition[55] between the higher-order topological insulators, metal, and insulators by using the convolutional neural network method. However, no attention has been paid to whether there is a phase transition between the higher-order topological states and other topological phases.

In this paper, we study the phase transition of magnetic higher-order topological insulators in a disordered environment via machine learning. Combined with the noncommutative geometric method, we compare the similarities and differences of the phase diagrams. The stability of the higher-order topological insulators under weak disorder is obtained and our results are consistent with the previous study.[55] Furthermore, the phase diagram calculated by the convolutional neural network presents the phase transition from the normal insulator to the Chern insulator and from the higher-order topological insulator to the Chern insulator. By comparing the Chern number distribution, we find that the phase transition from the normal insulator to the Chern insulator does exist, which is consistent with the results of deep learning. However, there exists no disorder induced transition from the higher-order topological insulator to the Chern insulator. This result indicates the limitation of deep learning as well.

2. Higher-order topological insulator

Compared with the traditional topological insulators, higher-order topological states have edge (bound) states of $(d-n)$ dimensions protected by the topological symmetry, where d is the dimension of the system and n is the order of the second-order topological states. Taking a two-dimensional topological insulator as an example,[4] its Hamiltonian can be derived from a three-dimensional topological insulator and written as

$$H_{\mathrm{TI}} = \left(m + t\sum_i \cos k_i\right)\tau_z\sigma_0 + \lambda\sum_i \sin k_i \tau_x\sigma_i + H_{\mathrm{w}}, \quad (1)$$

where $i = x, y$ and τ, σ correspond to Pauli matrices on orbital and spin spaces, respectively, m is the mass term, and H_{w} represents the Anderson disorder. When $\lambda = 0$, $\pm(m + t\cos k_x + t\cos k_y)$ appears accidental degeneracy and the cross points are not located at the high symmetric point. The degeneracy in the energy spectrum will be removed by the coupling term for $\lambda \neq 0$. Then, a non-trivial topological insulator with a one-dimensional gapless topological edge state will be obtained. Firstly, in order to realize the second-order topological state, the edge state should be gapped with a newly introduced time-reversal-symmetry-broken term[17]

$$H_\Delta = \Delta(\cos k_x - \cos k_y)\tau_y\sigma_0, \quad (2)$$

when $k_x \neq k_y$, H_Δ is not zero. The time reversal symmetry of the system is destroyed, and the edge state is gapped, which causes a band gap at the edge states. With the evolution of k_x, k_y, the sign of H_Δ will be reversed, which means that the mass domain wall will appear on the limited sample edge. Thus, a bound state forms at the corner of the sample and it is a second-order topological insulating state with $n = 2$. Then, in order to study the change of the magnetic second-order topological state, a zeeman splitting term induced by magnetization is introduced[22]

$$H_{\mathrm{Z}} = B\tau_0\sigma_z, \quad (3)$$

where B is the magnetic field. Now, the phase diagram varying with B and the mass term m in a clean sample can be obtained. According to the band gap closure conditions at four high symmetric points[22] $(0,0), (0,\pi), (\pi,0), (\pi,\pi)$, the phase boundaries satisfy the following relation:

$$\begin{aligned} &2t + m \pm B = 0,\\ &-2t - m \pm B = 0,\\ &2t - m \pm B = 0,\\ &-2t + m \pm B = 0. \end{aligned} \quad (4)$$

Other parameters are set as $t = 1$, $\Delta = t/4$, $\lambda = t$, so the phase boundary can be determined. As shown in Fig. 1, when $B = 0$, there exist two different phases corresponding to the second-order topological insulators ($|m| < 2t$) and the normal insulators ($|m| > 2t$).

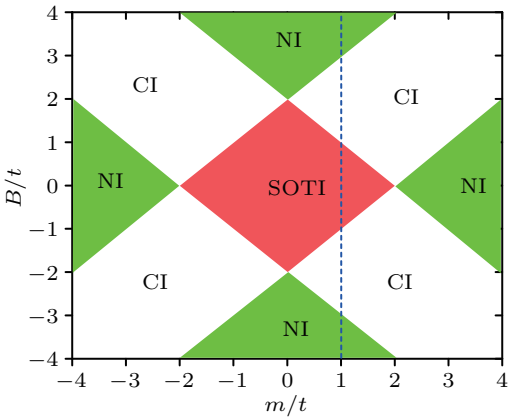


Fig. 1. Clean sample phase diagram. The horizontal axis is the mass term m and the vertical axis is the magnetic field B. Here, the green, white, and red areas correspond to the normal insulator (NI), Chern insulator (CI), and second-order topological insulator (SOTI), respectively. The blue dotted line in the figure is $m = t$. Magnetic field B is within $[-4t, 4t]$. Other parameters in this article are all set to $t = 1$, $\Delta = t/4$, and $\lambda = t$.

The zeeman term induces band gap closure and introduces a third phase: Chern insulator (CI). In order to obtain the eigenstates and eigenvalues under the finite size condition, the discretization method with $\cos ka = (\mathrm{e}^{\mathrm{i}ka} + \mathrm{e}^{-\mathrm{i}ka})/2$ and

$\sin ka = (e^{ika} - e^{-ika})/(2i)$ is used, where a is the lattice constant. We set $a = 1$ for simplicity. Then, the Hamiltonian can be rewritten in a tight-binding form as

$$H = T_0 a_i^\dagger a_i + T_x a_{i+\delta x}^\dagger a_i + T_y a_{i+\delta y}^\dagger a_i + \text{H.C.} \tag{5}$$

Here, a_i ($a_i^\dagger$) represent the four annihilation (creation) operators of point i, which has four orbital degrees of freedom. The on-site potential matrix is $T_0 = m\tau_z\sigma_0 + B\tau_0\sigma_z + \varepsilon_i\tau_0\sigma_0$, and ε_i represents the Anderson disorder, which randomly distributes in $[-W/2,\ W/2]$. The x-direction and y-direction hopping matrices are $T_x = \frac{t}{2}\tau_z\sigma_0 + \frac{\lambda}{2i}\tau_x\sigma_x + \frac{\Delta}{2}\tau_y\sigma_0$ and $T_y = \frac{t}{2}\tau_z\sigma_0 + \frac{\lambda}{2i}\tau_x\sigma_y - \frac{\Delta}{2}\tau_y\sigma_0$, respectively.

We choose the position of the blue dotted line shown in Fig. 1 ($m = t$) to get the phase transition of the second-order topological states. In order to confirm the phases with different magnetic field B, the band structure of a nanoribbon along x-axis is plotted in Fig. 2 [see Figs. 2(a)–2(c)]. Although the edge states still exist for $B = 0$, the curves are gapped. This is because the H_Δ term breaks the time reversal symmetry and makes the topological insulator become a second-order topological insulator. When the magnetic field increases, the band gap of the edge states closes when $B = 2t$. Subsequent calculations indicate that the Chern number at this location is quantized [Chern number = 1, see Fig. 6]. As the magnetic field continues to increase to $B = 4t$ in Fig. 2(c), the edge state finally disappears while the bulk gap still exists, which corresponds to the normal insulator. In order to examine the existence of the second-order topological states, we also calculate the eigenvalue evolution with the variation of magnetic field B for a 32×32 square sample in Fig. 2(d). When $|m| < 0.7t$, zero energy states appear [see Fig. 2(d)]. Due to the finite size effect, the range of zero energy states is less than the theoretical prediction $|m| < t$. In a word, these results are consistent with the phase diagram shown in Fig. 1.

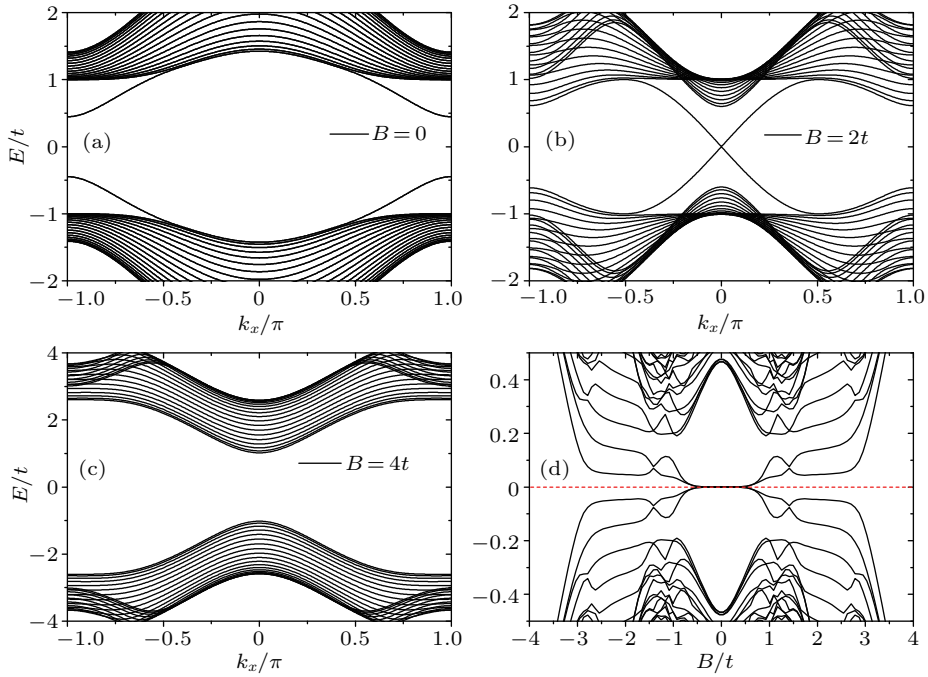


Fig. 2. The energy band distributions under different magnetic fields: (a) $B = 0$ (second-order topological insulators), (b) $B = 2t$ (Chern insulators), (c) $B = 4t$ (normal insulators). (d) The evolution of energy levels with B for a square system with the size of 32×32.

Previous research[55] mostly focused on on the stability of the second-order topological states with disorder and the transition between the metal and insulator phases. In the next section, we investigate whether the second-order topological insulator can transit into the Chern insulator by a machine learning method.

3. Phase diagram calculated by machine learning method

In this section, we briefly introduce the structure of the convolutional neural network adopted in our work. Since there exist only three cases [see Fig. 4] for clean samples, Lenet-5 convolutional neural network framework[45] is adopted. We construct the neural network with the help of Tensorflow. The entire neural network is composed of two convolution layers, two full connection layers, and an output layer. In addition to the output layer, we select Relu as the activation function. Since the wave function is a grayscale graph without RGB value, we use four convolution kernels with the kernel size $5 \times 5 \times 1$ (5×5 corresponds to the width and 1 indicates the depth) at the beginning. The output of the convolution layer is pooled immediately afterwards. If not specified, the convolution step size defaults to 1 and the pooling kernel size defaults to 2 with pooling step set to 2. On the second layer, we select

eight convolution kernels with kernel size $5 \times 5 \times 4$ instead. Batch normalization is introduced after pooling to adjust the data structures. The results of the convolution layer are input into the full connection layer. We choose two full connection layers by using 80 and 32 neurons, respectively. The output layer has 3 outputs and the activation function is softmax. The outputs of the final layer are the normalized probability and the corresponding labels of the maximum probability, in other words, the Chern insulator, the second-order topological insulator, and the normal insulator. First, we select the blue line position as shown in Fig. 1 to generate the training and test data. B distributes in $[-4t,\ 4t]$. Then, 20000 groups of B are randomly selected and the corresponding wave functions are calculated. Subsequently, different labels are attached according to the value of B ($|B| < t$, corresponding to the second-order topological insulator; $t \leq |B| < 3t$, corresponding to the Chern insulator; otherwise, considered as the normal insulator). Figures 3(a)–3(c) show the wave function distributions of the Chern insulator, the normal insulator, and the second-order topological insulator, respectively. For the normal insulators, the density of state is mainly concentrated in the center of the square sample as shown in Fig. 3(b). While the the Chern insulator [Fig. 3(a)] has an edge state, where the wave function is distributed in the interface with vacuum. For the second-order topological insulators, because of the corner states in the band gap of the edge states [Fig. 3(c)], the spectrum of this state is closer to the Fermi energy than that of the edge state. This means we can distinguish these different phases by the wave function distributions, which is also an important basis for deep learning classification. We choose the wave function of the eigenvalue (below and closest to the Fermi surface) as the final input wave function. 20000 sets of data are divided into 15000 sets of training data and 5000 sets of testing data. After 100 rounds of training, we confirm that the accuracy of the network has reached 99.99% and stop the training. Then, within the same range of $[-4t,\ 4t]$ for B, the disordered W is gradually increased and the disordered wave function is generated. Afterwards, the disordered wave functions (after being averaged 40 times) are imported into the trained network. Then, the final result is obtained.

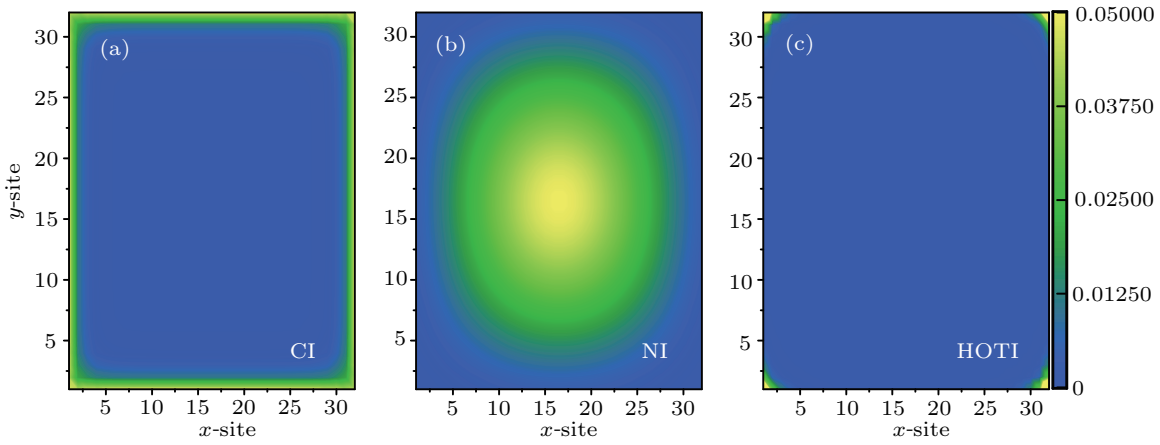


Fig. 3. The wave function distributions of different phases. (a) Chern insulator, the density of states is located around the edge. (b) Normal insulator, there is no state at the edge. (c) Second-order topological insulator, which has a density of state peak corresponding to a zero-dimensional bound state at the four corners of the square. The sample size is 32×32.

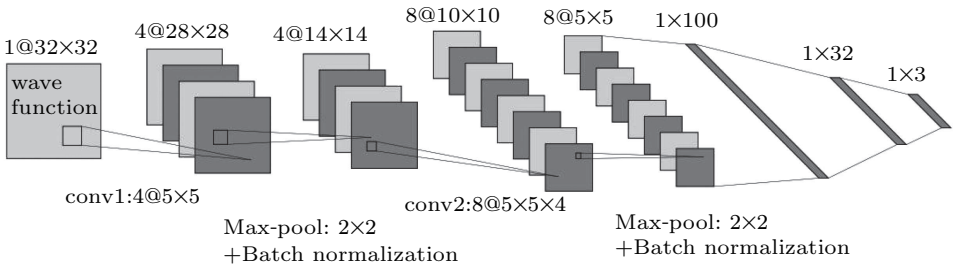


Fig. 4. Neural network structure. The input is the real space wave function distribution. There exist two layers of convolution and two layers of full connection to reach the output layer. The size of the convolution kernel and the number of neurons in the full connection layer are marked in the figure.

Figure 5 shows the output of the trained neural network by using the disordered wave function as the input, where the vertical axis is the magnetic field B and the horizontal axis is the disorder strength W. Since the wave function under strong disorder may produce a completely different distribution from the training samples, we only select the disorder strength of $0 \leq W \leq 5t$.

Figures 5(a) and 5(b) show the maximum probability of the output of the neural network and the corresponding phase of the maximum probability, respectively. Firstly, the prob-

ability distribution of most areas is higher than 99%, which indicates that the network training is consistent with expectation. Furthermore, the probability of the phase boundary is about 50%, which is significantly lower than the probability on its both sides. This is due to the fact that the phase boundary may have the features of two different phases, so the network cannot give a high probability for either of the two phases.Secondly, we pay attention to the phase diagram in Fig. 5(b). When $B = 0$, the topological state of second-order is not affected by the disorder strength as large as $W = 3.5t$. However, with the increase of magnetic field B, the stability of the topological state is slightly weakened. This system also exists a topological Anderson transition induced by disorder, which indicates a phase transition from the normal insulator to the Chern insulator [see the red line in Fig. 5(a)]. Moreover, the network suggests that there exists a phase transition from the second-order topological insulator to the Chern insulator. Since our training process only contains three phases (two of them are the topological nontrivial phases), a comparison between Fig. 5 and other results is also needed to determine whether the judgment of the two phase transitions (the normal insulator to the Chern insulator and the second-order insulator to the Chern insulator) is correct or not.

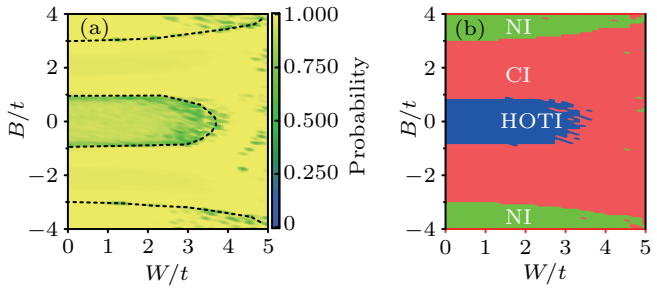


Fig. 5. (a) The maximum probability of the output determined by the machine verses B and W. The dotted black line is the phase boundary depicted by the minimum probability. (b) The corresponding phase with the maximum probability in plane B–W. Red, green, and blue parts correspond to the Chern insulator, normal insulator, and second-order topological insulator, respectively.

4. Chern-number analysis

In this part, we will use the non-commutative geometry method to calculate the Chern number of disordered samples. The difference of phase diagram obtained by non-commutative geometry and deep learning method is also be investigated.

We firstly give a brief review of the Chern number calculation based on non-commutative geometric method.[56–61] According to the perturbation theory, the Chern number of an infinite system can be expressed as follows:

$$C = \frac{1}{2\pi \mathrm{i}} \int_{\mathrm{BZ}} \mathrm{Tr}\{P_{\boldsymbol{k}}[\partial_{k_x} P_{\boldsymbol{k}}, \partial_{k_y} P_{\boldsymbol{k}}]\}, \tag{6}$$

where $P(\boldsymbol{k})$ corresponds to projection operators for all occupied states and k_x, k_y present the momentum of x and y direction, respectively. Consider k_x, k_y as discrete ones. The Brillouin zone is divided into $N \times N$ grid and $\boldsymbol{k}_n = (n_1\Delta, n_2\Delta)$ with $n_{1,2} = 1, \ldots, N$ and $\Delta = 2\pi/N$. Since the discretization makes the brillouin zone discontinuous, the integration can be expressed as

$$\int \mathrm{d}\boldsymbol{k} = \sum_{\boldsymbol{k}_n} \Delta^2. \tag{7}$$

In the whole calculation process, the most important step is to calculate $\partial_{k_i} P_{\boldsymbol{k}}$. The analytic solution in the continuous momentum space can be easily obtained with the help of momentum(k_x, k_y) dependent eigenvalue. For the discrete momentum space, $\partial_{k_i} P_{\boldsymbol{k}}$ should be calculated according to the definition of differentiation

$$\partial_{k_i} P_{\boldsymbol{k}} \to \delta_{k_i} P_{\boldsymbol{k}_n} = \sum_{m=1}^{Q} c_m [P_{\boldsymbol{k}_n + m\Delta_i} - P_{\boldsymbol{k}_n - m\Delta_i}], \tag{8}$$

where $\Delta_1 = (\Delta, 0)$, $\Delta_2 = (0, \Delta)$, and Q can take arbitrary value between 0 and $N/2$. For infinite system, the space projection operator is the continuous function in momentum space and should satisfy the following form $P_{\boldsymbol{k}} = \sum_{n \varepsilon T^2} b_n \mathrm{e}^{\mathrm{i}\boldsymbol{k}n}$. Therefore, we only need to find the approximation form of $\mathrm{e}^{\mathrm{i}\boldsymbol{k}x}$ in differential form, which can be written as

$$(\partial_{k_i} - \delta_{k_i})\mathrm{e}^{\mathrm{i}\boldsymbol{k}x} = \mathrm{i}\left[x_i - 2\sum_{m=1}^{Q} c_m \sin(m\Delta x_i)\right]\mathrm{e}^{\mathrm{i}\boldsymbol{k}x}. \tag{9}$$

c_m is a vector $\boldsymbol{c} = (c_1, c_2, \ldots, c_Q)$. Then, we perform Taylor expansion on $\sin(m\Delta x_i)$ to the order of δ^{2Q}, where x_1 (x_2) correspond to x, (y) direction. Thus, $\boldsymbol{c}$ must satisfy the following equation in order to let $x_i - 2\sum_{m=1}^{Q} c_m \sin(m\Delta x_i) = 0$:

$$\boldsymbol{A}\boldsymbol{c}^{\mathrm{T}} = \frac{2}{\Delta}(1, 0, 0, \cdots, 0)^{\mathrm{T}}, \tag{10}$$

where $A_{ij} = j^{2i-1}$ with $i, j = 1, 2, \ldots Q$. Now, the expansion coefficient c_m is obtained and $(\partial_{k_i} - \delta_{k_i})\mathrm{e}^{\mathrm{i}\boldsymbol{k}x} = 0$ is satisfied to Δ^{2Q} order. These results are determined by (k_x, k_y), but the Chern number for dirty samples is based on a discrete lattice model with finite size. In real space, we have $\delta_{k_i} P_{\boldsymbol{k}} = -\mathrm{i}[x_i, P]$ after turning $\mathrm{i}\partial_{k_x}$ $(\mathrm{i}\partial_{k_y})$ into $x(y)$. Then, $\delta_{k_i} P_{\boldsymbol{k}}$ can be rewritten as

$$[x_i, P] = \mathrm{i}\sum_{m=1}^{Q} c_m (\mathrm{e}^{-\mathrm{i}m\boldsymbol{x}\Delta_i} P \mathrm{e}^{\mathrm{i}m\boldsymbol{x}\Delta_i} - \mathrm{e}^{\mathrm{i}m\boldsymbol{x}\Delta_i} P \mathrm{e}^{-\mathrm{i}m\boldsymbol{x}\Delta_i}). \tag{11}$$

Therefore, the Chern number in real space can be rewritten as

$$C = -\frac{2\pi \mathrm{i}}{N^2} \sum_{n,\alpha} \langle n, \alpha | P[-\mathrm{i}[x_1, P], -\mathrm{i}[x_2, P]] | n, \alpha \rangle, \tag{12}$$

where P is the projection operator of occupied states on the basis of real space and $|n, \alpha\rangle$ is the real space coordinates. When the real space coordinate $\boldsymbol{x}$ is acting on $|n, \alpha\rangle$, the corresponding space coordinates will be obtained. The index theory shows that the Chern number should be quantized as long as the Fermi surface locates in the bulk gap (not caused by the

discretization momentum because of finite size effect). Futhermore, the quantized Chern number even varies with the existence of the bulk gap.

Based on the real space calculation, we obtain both the Chern number for clean samples and the evolution of the Chern number under the variation of disorder strength for dirty samples. As shown in Fig. 6, the system has the Chern number of quantized $C = 1$ in the range of $t < |B| < 3t$ for clean samples. This region corresponds to the Chern insulator. In addition, the Chern number changes from $C = 0$ to $C = 1$ with the increase of disorder strength W for $|B| > 3t$. Thus, the topological Anderson phase transition (the normal insulator to the Chern insulator) is confirmed, which agrees with the result obtained through the convolutional neural network. Finally, the region of $|B| < t$ that we most concerned corresponds to the second-order topological insulator. However, no quantization is obtained by increasing W in this region, and the area of quantization is much smaller than the result achieved through machine learning [the Chern insulator region in Fig. 5(b)].

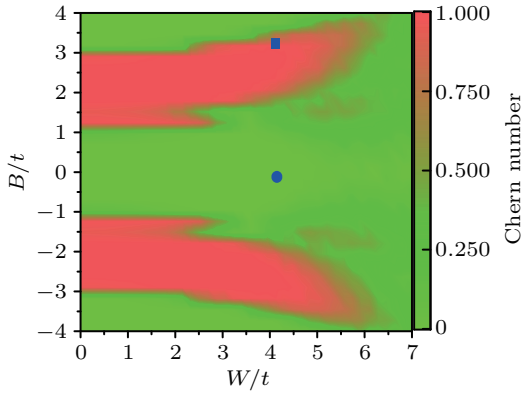


Fig. 6. Chern number projection obtained by noncommutative geometry. The horizontal axis is the magnetic field intensity B and the vertical axis is the disordered intensity W. Here, we take the absolute value of the Chern number. Because whether the Chern number takes positive or negative value, the system is a Chern insulator.

In order to explain this contradiction between the two different methods, we make a brief discussion below. We present the wave functions corresponding to the two marked points (square and circle) in Fig. 6. Figure 7(a) shows the wave function distribution for the square symbol marked in Fig. 6, where the Anderson disorder turns the normal insulator into the Chern insulator. It has obvious edge state characteristics. Even though the wave function distribution is much different from that in Fig. 3(a), the neural network can still present a correct result. However, the wave function [see Fig. 7(b)] still holds the feature of edge state, although the Chern number at this point is not quantized [marked by circle in Fig. 6]. This means the edge state without quantized Chern number is not the edge state of the Chern insulator, though the wave function distribution is very similar to the Chern insulator one.

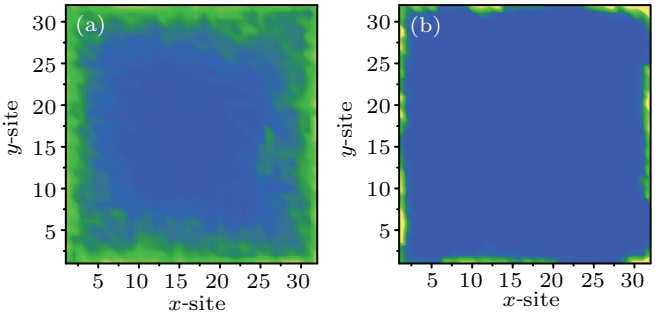


Fig. 7. (a) The wave function distribution diagram of the marked square (the point from Chern insulator to normal insulator) in Fig. 6. (b) The wave function distribution diagram of the marked circle (the point from Chern insulator to second-order topological insulator) in Fig. 6.

In order to explain the emergence of the edge state distribution, we investigate the wave function distribution in detail [see Figs. 8(a)–8(c)]. In the previous calculation, each wave function distribution was plotted by the average of 40 individual wave function distribution diagrams. In Figs. 8(a)–8(c), we directly take only one disordered sample and get the wave function distribution. By randomly resetting the disorder for three times, we get three random wave function distributions. It can be seen that there are bound states in Figs. 8(a)–8(c), which are all at the boundary, although they are not at the same position. This result means that the position of the bound states at the boundary can be random. We use dashed red lines to duplicate the bound states of Figs. 8(b) and 8(c) into Fig. 8(a). Obviously, the region of the bound state at the boundary will be larger than the result of any one graph after averaging the sum of the three graphs. Therefore, if more are added during the calculation, there is a high probability of producing a wave function distribution similar to that of the edge state of the Chern insulator. This is the most likely reason for misjudgment.

In order to confirm whether there is a phase transition, we use the self-consistent Born approximation method[38,39] to calculate the evolution of the bulk gap with disorder. The self-consistent Born approximation is based on the following formula:

$$\Sigma_{\mathrm{d}} = \frac{W^2}{48\pi^2}\int_{\mathrm{BZ}} \mathrm{d}k[E_{\mathrm{F}} + \mathrm{i}0^+ - H(k) - \Sigma_{\mathrm{d}}]^{-1}, \qquad (13)$$

where Σ_{d} is the self-energy caused by disorder, W is the disorder strength, E_{F} is the Fermi level, and $H(k) = H_{\mathrm{TI}} + H_{\Delta} + H_{\mathrm{Z}}$. The parameters are the same as those in Fig. 7 with $B = 0$. By solving Eq. (13), we obtain Σ_{d} and the renormalized Hamiltonian $\Sigma_{\mathrm{d}} + H(k)$. Based on the renormalized Hamiltonian, the evolution of the bulk gap versus disorder W is obtained, as shown in Fig. 8(d). The bulk band gap increases at the beginning and then decreases. However, the bulk gap exists during the whole process, which means that the system does not undergo a phase transition. Thus, we infer that figures 8(a)–8(c) are still in the higher-order topological insulator phase.

The reason for the shift of the bound states in space may be that the corner state of the higher-order topological insulator is very sensitive to the localized on-site energy. Due to randomness of disorder, the on-site energy of a certain position is higher and the on-site energy of another certain position is lower, so the bound state will move in space, thus forming the effect of edge state after averaging the individual wave function distributions.

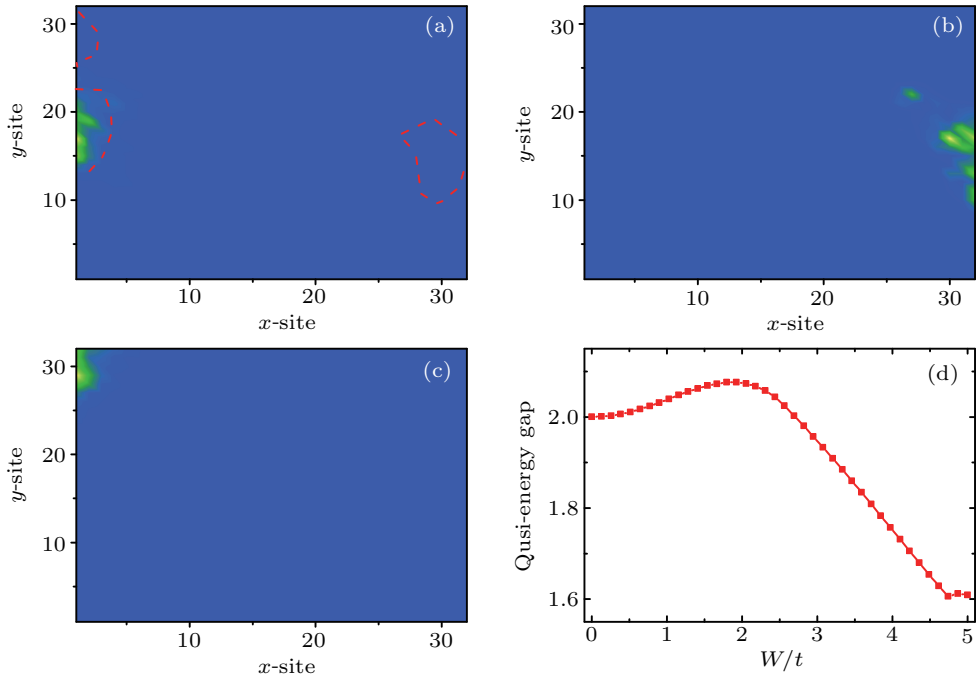


Fig. 8. (a)–(c) The wave function distributions of three random disordered samples. (d) The evolution of the bulk band gap versus disorder.

5. Conclusion

In summary, we studied the disordered phase transition of the magnetic second-order topological insulators using the deep learning method. We found that the second-order topological states are stable when the disorder strength satisfies $W \leq 3.5t$ and the neural network can accurately judge the topological Anderson phase transition from the normal insulator to the Chern insulator. However, by comparing the Chern number under disordered conditions through the non-commutative geometry method, we found that although the neural network predicts a transition from the second-order topological state to the Chern insulator, such phase transition does not happen actually. This anomaly originates from the fact that for the second-order topological insulator, the bound states randomly appear at the edge of the sample under the strong disorder. After the ensemble average, the averaged bound states make the wave function distributions capture the edge state feature, while it is absent for the individual samples.

Acknowledgment

We are grateful to C. Z. Chen for helpful discussions.

References

[1] Klitzing K V 1986 *Rev. Mod. Phys.* **58** 519
[2] Tong D 2016 arxiv 1606.06687
[3] Hasan M Z and Kane C L 2010 *Rev. Mod. Phys.* **82** 3045
[4] Qi X L and Zhang S C 2011 *Rev. Mod. Phys.* **83** 1057
[5] Deng H X, Song Z G, Li S S, Wei S H and Luo J W 2018 *Chin. Phys. Lett.* **35** 057301
[6] Gong Y, Guo J, Li J, *et al.* 2019 *Chin. Phys. Lett.* **36** 076801
[7] He K, Ma X C, Chen X, Lu L, Wang Y Y and Xue Q K 2013 *Chin. Phys. B* **22** 067305
[8] Yang Z Q, Jia J F and Qian D 2016 *Chin. Phys. B* **25** 117312
[9] Lv B Q, Weng H M, Fu B B, Wang X P, Miao H, Ma J, Richard P, Huang X C, Zhao L X, Chen G F, Fang Z, Dai X, Qian T and Ding H 2015 *Phys. Rev. X* **5** 031013
[10] Xu X Y, Belopolski I, Alidoust N, Neupane M, Bian G, Zhang C L, Sankar R, Chang G Q, Yuan Z J, Lee C C, Huang S M, Zheng H, Ma J, Sanchez D S, Wang B K, Bansil A, Chou F C, Shibayev P P, Lin H, Jia S and Hasan M Z 2015 *Science* **349** 613
[11] Fu L and Kane C L 2008 *Phys. Rev. Lett.* **100** 096407
[12] Qi K L, Hughes T L and Zhang S C 2010 *Phys. Rev. B* **82** 184516
[13] Alicea J 2010 *Rep. Prog. Phys.* **75** 076501
[14] Li Y H, Liu J, Song J T, Jiang H, Sun Q F and Xie X C 2018 *Sci. China. Phys. Mech.* **61** 97411
[15] Qi X L, Hughes T L and Zhang S C 2008 *Phys. Rev. B* **78** 195424
[16] Li R, Wang J, Qi X L and Zhang S C 2010 *Nat. Phys.* **6** 284
[17] Schindler F, Cook A M, Vergniory M G, Wang Z J, Parkin S P, Andrei Bernevig B and Neupert T 2018 *Sci. Adv.* **4** 0346
[18] Ezawa M 2018 *Phys. Rev. B* **98** 045125
[19] Ezawa M 2018 *Phys. Rev. Lett.* **120** 026801
[20] Langbehn J, Peng Y, Trifunovic L, Oppen F V and Brouwer P W 2017 *Phys. Rev. Lett.* **119** 246401
[21] Song Z, Fang Z and Fang C 2017 *Phys. Rev. Lett.* **119** 246402
[22] Ezawa M 2018 *Phys. Rev. B* **97** 155305
[23] Yang Y, Jia Z Y, Wu Y, Hang Z H, Jiang H and Xie X C 2019 arxiv: 1903.01816
[24] Benalcazar W A, Bernevig B A and Hughes T L 2017 *Science* **357** 61
[25] Garcia M S, Peri V, Süsstrunk R, Bilal O R, Larsen T, Villanueva L G and Huber S D 2018 *Nature* **555** 342

[26] Xue H R, Yang Y H, Gao F, Chong Y D and Zhang B L 2019 *Nat. Mater.* **18** 108

[27] Zhang X, Wang H X, Lin Z K, Tian Y, Xie B Y, Lu M H, Chen Y F and Jiang J H 2018 arxiv: 1806.10028

[28] Imhof S, Berger C, Bayer F, Brehm J, Molenkamp LW, Kiessling T,Schindler F, Lee C H, Greiter M, Neupert T and Thomale R 2018 *Nat. Phys.* **14** 925

[29] Li J, Chu R L, Jain J K and Shen S Q 2009 *Phys. Rev. Lett.* **102** 136806

[30] Jiang H, Wang L, Sun Q F and Xie X C 2009 *Phys. Rev. B* **80** 165316

[31] Chen R, Xu D H and Zhou B 2019 arXiv:1907.05724

[32] Zhang Z Q, Wu B L, Song J and Hua Jiang 2019 arXiv:1906.04064

[33] Zhang D W, Tang L Z, Lang L J, Yan H and Zhu S L 2019 arXiv:1908.01172

[34] Chen C Z, Song J T, Jiang H, Sun Q F, Wang Z Q and Xie X C 2015 *Phys. Rev. Lett.* **115** 246603

[35] Song J T, Liu H W, Jiang H, Sun Q F and Xie X C 2012 *Phys. Rev. B* **85** 195125

[36] Chen C Z, Liu H W, Jiang H and Xie X C 2016 *Phys. Rev. B* **93** 165420

[37] Song J T and Prodan E 2014 *Phys. Rev. B* **89** 224203

[38] Chen C Z, Liu H W and Xie X C 2019 *Phys. Rev. Lett.* **122** 026601

[39] Wu Y J, Liu H W, Jiang H and Xie X C 2017 *Phys. Rev. B* **96** 024201

[40] Prodan E, Hughes T L and Bernevig B A 2010 *Phys. Rev. Lett.* **105** 115501

[41] Mondragon-Shem I, Hughes T L, Song J T and Prodan E 2014 *Phys. Rev. Lett.* **113** 046802

[42] Nomura K and Nagaosa N 2011 *Phys. Rev. Lett.* **106** 166802

[43] Wu B L, Song J T, Zhou J J and Jiang H 2016 *Chin. Phys. B* **25** 117311

[44] Guo H M, Rosenberg G, Refael G and Franz M 2010 *Phys. Rev. Lett.* **105** 216601

[45] LeCun Y 2015 http://yann.lecun.com/exdb/lenet 20

[46] Deng D L, Li X and Sarma S D 2017 *Phys. Rev. B* **96** 195145

[47] Zhang Y and Kim E A 2017 *Phys. Rev. Lett.* **118** 216401

[48] Morii M, Ikeda S, Tominaga N, Tanaka M, Morokuma T, Ishiguro K, Yamato J, Ueda N, Suzuki N, Yasuda N and Yoshida N 2016 *Publ. Astron. Soc. Jan.* **68**

[49] Carrasquilla J and Melko R G 2017 *Nat. Phys.* **13** 431

[50] Li R, Liu Y, Zuo S L, Zhao T Y, Hu F X, Sun J R and Shen B G 2018 *Chin. Phys. B* **27** 047501

[51] Miao J Y 2019 *Chin. Phys. Lett.* **36** 097501

[52] Zhang B, Zheng X Q, Zhao T Y, Hu F X, Sun J R and Shen B G 2018 *Chin. Phys. B* **27** 067503

[53] Yao T S, Tang C Y, Yang M, Zhu K J, Yan D Y, Yi C J, Feng Z L, Lei H C, Li C H, Wang L, Wang L, Shi Y G, Sun Y J and Ding H 2019 *Chin. Phys. Lett.* **36** 068101

[54] Carleo G, Cirac I, Cranmer K, Daudet L, Schuld M, Tishby N, Vogt-Maranto L and Zdeborová L 2019 arXiv: 1903.10563

[55] Araki H, Mizoguchi T and Hatsugai Y 2019 *Phys. Rev. B* **99** 085406

[56] Loring T A and Hastings M B 2011 *Euro. Phys. Lett.* **92** 67004

[57] Prodan E 2011 *J. Phys. A-Math. Theor.* **44** 113001

[58] Hastings M B and Loring T A 2011 *Ann. Phys.* **326** 1699

[59] Zhang Y F, Yang Y Y, Ju Y, Sheng L, Shen R, Sheng D N and Xing D Y 2013 *Chin. Phys. B* **22** 117312

[60] Sheng L, Li H C, Yang Y Y, Sheng D N and Xing D Y 2011 *Chin. Phys. B* **22** 067201

[61] Kitaev A 2006 *Ann. Phys.* **321** 2